

Macrocyclic effects upon isomeric $\text{Cu}^{\text{II}}\text{M}^{\text{II}}$ and $\text{M}^{\text{II}}\text{Cu}^{\text{II}}$ cores. Formation with unsymmetric phenol-based macrocyclic ligands

MASAMI YONEMURA, YUUKI NAKAMURA, NAOKI USUKI and
HISASHI ŌKAWA*

Department of Chemistry, Faculty of Science, Kyushu University, Hakozaki,
Higashiku 6-10-1, Fukuoka 812-8581, Japan

Abstract. This paper discusses coordination-position isomeric $\text{M}^{\text{II}}\text{Cu}^{\text{II}}$ and $\text{Cu}^{\text{II}}\text{M}^{\text{II}}$ complexes, using unsymmetric dinucleating macrocycles ($\text{L}^{\text{m,n}}$)²⁻ ($\text{L}^{2;2}$)²⁻, ($\text{L}^{2;3}$)²⁻ and ($\text{L}^{2;4}$)²⁻) that comprise two 2-(N-methyl)-aminomethyl-6-iminomethyl-4-bromophenolate entities, combined through the ethylene chain ($m = 2$) between the two amine nitrogens and through the ethylene, trimethylene or tetramethylene chain ($n = 2, 3$ or 4) between the two imine nitrogens. The macrocycles have dissimilar N(amine)₂O₂ and N(imine)₂O₂ metal-binding sites sharing the phenolic oxygens. The reaction of the mononuclear Cu^{II} precursors, [$\text{Cu}(\text{L}^{2;2})$], [$\text{Cu}(\text{L}^{2;3})$] and [$\text{Cu}(\text{L}^{2;4})$], with a M^{II} perchlorate and a M^{II} acetate salt formed (acetato) $\text{M}^{\text{II}}\text{Cu}^{\text{II}}$ complexes: [$\text{CoCu}(\text{L}^{2;2})(\text{AcO})\text{ClO}_4 \cdot 0.5\text{H}_2\text{O}$] (**1**), [$\text{NiCu}(\text{L}^{2;2})(\text{AcO})\text{ClO}_4$] (**2**), [$\text{ZnCu}(\text{L}^{2;2})(\text{AcO})\text{ClO}_4$] (**3**), [$\text{CoCu}(\text{L}^{2;3})(\text{AcO})\text{ClO}_4 \cdot 0.5\text{H}_2\text{O}$] (**4**), [$\text{NiCu}(\text{L}^{2;3})(\text{AcO})\text{ClO}_4$] (**5**), [$\text{ZnCu}(\text{L}^{2;3})(\text{AcO})\text{ClO}_4 \cdot 0.5\text{H}_2\text{O}$] (**6**), [$\text{CoCu}(\text{L}^{2;4})(\text{AcO})(\text{DMF})\text{ClO}_4$] (**7**), [$\text{NiCu}(\text{L}^{2;4})(\text{AcO})\text{ClO}_4 \cdot 2\text{DMF}$] (**8**) and [$\text{ZnCu}(\text{L}^{2;4})(\text{AcO})\text{ClO}_4$] (**9**) (the formulation [$\text{M}_a\text{M}_b(\text{L}^{\text{m,n}})$]²⁺ means that M_a resides in the aminic site and M_b in the iminic site). The site selectivity of the metal ions is demonstrated by X-ray crystallographic studies for 2-MeOH, **3**, **5**, **7**, and **9**. An (acetato) $\text{Cu}^{\text{II}}\text{Zn}^{\text{II}}$ complex, [$\text{CuZn}(\text{L}^{2;3})(\text{AcO})\text{ClO}_4$] (**10**), was obtained by the reaction of [$\text{PbCu}(\text{L}^{2;3})$](ClO_4)₂ with $\text{ZnSO}_4 \cdot 4\text{H}_2\text{O}$, in the presence of sodium acetate. Other complexes of the $\text{Cu}^{\text{II}}\text{M}^{\text{II}}$ type were thermodynamically unstable to cause a scrambling of metal ions. The Cu migration from the iminic site to the aminic site in the synthesis of **10** is explained by the 'kinetic macrocyclic effect'. The coordination-position isomers, **6** and **10**, are differentiated by physicochemical properties.

Keywords. Heterodinuclear complex; coordination-position isomers; macrocyclic effect; crystal structure.

1. Introduction

The design of dinucleating compartmental ligands, whose two metal-binding sites are unsymmetric with respect to the cavity size, coordination number, geometric requirement, or the nature of the donor atom, is important for the study of heterodinuclear complexes¹. For this purpose, we have developed the unsymmetric phenol-based macrocycles of the type in chart 1, having two dissimilar N(amine)₂O₂ and N(imine)₂O₂ metal-binding sites sharing the bridging phenolic oxygens²⁻⁴. They are abbreviated as ($\text{L}^{\text{m,n}}$)²⁻ using the methylene number m between the amine nitrogens and the methylene number n between the imine nitrogens. Analogous macrocycles bearing a pyridyl auxiliary at the amine nitrogens⁵ or doubly bridged

*For correspondence

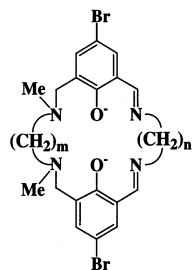
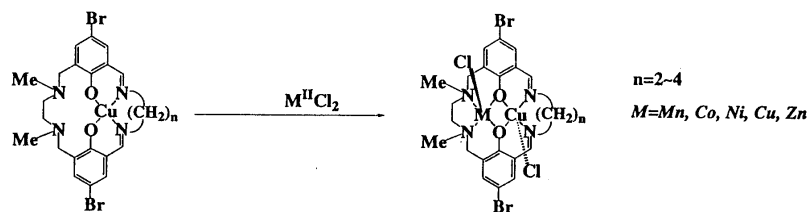
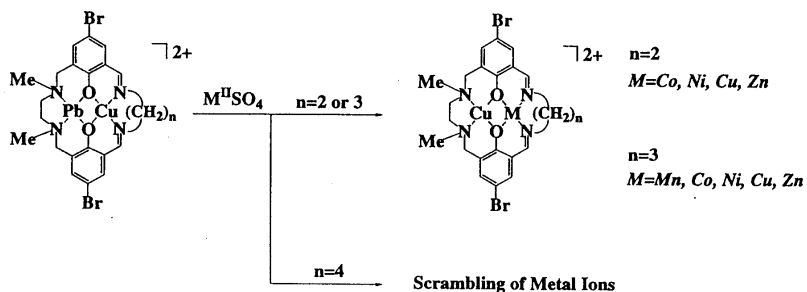


Chart 1. Chemical structure of $(L^{m:n})^{2-}$.

Method A



Method B



Scheme 1. Synthetic methods for heterodinuclear $M^{II}Cu^{II}$ and $Cu^{II}M^{II}$ complexes of $(L^{m:n})^{2-}$.

through two ethylene chains between the amine nitrogens⁶ were prepared in other laboratories.

Heterodinuclear $Cu^{II}M^{II}$ or $M^{II}Cu^{II}$ complexes of $(L^{2;2})^{2-}$, $(L^{2;3})^{2-}$ and $(L^{2;4})^{2-}$ can be derived by two different methods; (i) the reaction of the mononuclear Cu^{II} precursors $[Cu(L^{m:n})]$ (having the Cu^{II} in the iminic site) with M^{II} salts and (ii) the transmetalation of the Pb^{II} of the dinuclear $Pb^{II}Cu^{II}$ precursors $[PbCu(L^{m:n})](ClO_4)_2$ for M^{II} ions (scheme 1)²⁻⁴. The first method using M^{II} chloride salts gave $[MCu(L^{m:n})Cl_2]$ ($(L^{m:n})^{2-} = (L^{2;2})^{2-}$, $(L^{2;3})^{2-}$, $(L^{2;4})^{2-}$; $M = Mn^{II}$, Co^{II} , Ni^{II} , Zn^{II})^{2,4} that have the M^{II} in the $N(amine)_2O_2$

site and the Cu^{II} in the $\text{N}(\text{imine})_2\text{O}_2$ site: hereafter, the formulation $[\text{M}_a\text{M}_b(\text{L}^{m;n})]^{2+}$ means that M_a resides in the aminic site and M_b in the iminic site. The second method using M^{II} sulphate salts gives the $\text{Cu}^{\text{II}}\text{M}^{\text{II}}$ perchlorate complexes $[\text{CuM}(\text{L}^{m;n})](\text{ClO}_4)_2$ ($(\text{L}^{m;n})^{2-} = (\text{L}^{2;2})^{2-}$, $(\text{L}^{2;3})^{2-}$; $\text{M} = \text{Co}^{\text{II}}$, Ni^{II} , Zn^{II})³. In this synthesis, the Cu^{II} migrates from the iminic site to the aminic site and the M^{II} is accommodated in the iminic site.

Our previous studies suggest that isomeric $\text{M}^{\text{II}}\text{Cu}^{\text{II}}$ and $\text{Cu}^{\text{II}}\text{M}^{\text{II}}$ complexes (coordination-position isomers) can be derived from $(\text{L}^{m;n})^{2-}$ by taking advantage of the two synthetic methods, when an exogenous anionic donor is properly chosen. Coordination-position isomers consisting of two labile metal ions are very limited in spite of the great interest in basic coordination chemistry. In this work our aim was to provide isomeric (acetato) $\text{Cu}^{\text{II}}\text{M}^{\text{II}}$ and (acetato) $\text{M}^{\text{II}}\text{Cu}^{\text{II}}$ complexes of $(\text{L}^{2;2})^{2-} \sim (\text{L}^{2;4})^{2-}$. One of the latter class, $[\text{CuZn}(\text{L}^{2;3})(\text{AcO})](\text{ClO}_4)_2$, has been prepared from $[\text{PbCu}(\text{L}^{2;3})](\text{ClO}_4)_2$ by method **II** in the presence of acetate ion³.

2. Experimental

2.1 Preparation

The mononuclear Cu^{II} precursors, $[\text{Cu}(\text{L}^{2;2})]$, $[\text{Cu}(\text{L}^{2;3})]$ and $[\text{Cu}(\text{L}^{2;4})]$, and the dinuclear $\text{Pb}^{\text{II}}\text{Cu}^{\text{II}}$ precursors, $[\text{PbCu}(\text{L}^{2;2})](\text{ClO}_4)_2$, $[\text{PbCu}(\text{L}^{2;3})](\text{ClO}_4)_2$ and $[\text{PbCu}(\text{L}^{2;4})](\text{ClO}_4)_2$ were prepared by the methods described in our earlier papers².

2.1a (Acetato) $\text{M}^{\text{II}}\text{Cu}^{\text{II}}$ complexes: To a suspension of a mononuclear Cu^{II} precursor $[\text{Cu}(\text{L}^{m;n})]$ (1×10^{-4} mol) in methanol (10 cm^3) was added a methanol solution (15 cm^3) of a M^{II} perchlorate salt (5×10^{-5} mol) and a M^{II} acetate salt (5×10^{-5} mol), and the mixture was refluxed for 2 h. The resulting product was separated by filtration, washed with ether and dried *in vacuo*. The following complexes were obtained by this method (method I).

$[\text{CoCu}(\text{L}^{2;2})(\text{AcO})]\text{ClO}_4 \cdot 0.5\text{H}_2\text{O}$ (**1**). Green microcrystals. Found: C 34.74; H 3.29; N 6.85; Cu 8.08; Co 6.94%. Calcd. for $\text{C}_{24}\text{H}_{28}\text{Br}_2\text{ClCoCuN}_4\text{O}_{8.5}$: C 34.89; H 3.42; N 6.78; Cu 7.69; Co 7.13%. Selected IR [rcm^{-1}] using KBr: 1632, 1583, 1552, 1446, 1425, 1292, 1097, 1082, 764, 623. m_{ff} per CoCu: 4.69 m_{b} at 290 K. UV-Vis [I_{max}/nm ($\text{e}/\text{M}^{-1} \text{cm}^{-1}$)] in DMSO: 356 (8120), 542 (218).

$[\text{NiCu}(\text{L}^{2;2})(\text{AcO})]\text{ClO}_4$ (**2**). Green powder. Found: C 35.28; H 3.34; N 6.87; Cu 8.12; Ni 6.98%. Calcd. for $\text{C}_{24}\text{H}_{27}\text{Br}_2\text{ClCuN}_4\text{NiO}_8$: C 35.28; H 3.33; N 6.86; Cu 7.78; Ni 7.18%. Selected IR [rcm^{-1}] using KBr: 1632, 1583, 1445, 1292, 1098, 1083, 762, 624. m_{ff} per NiCu: 3.58 m_{b} at 290 K. UV-Vis [I_{max}/nm ($\text{e}/\text{M}^{-1} \text{cm}^{-1}$)] in DMSO: 355 (8290), 555 (170).

Single crystals of $[\text{NiCu}(\text{L}^{2;2})(\text{AcO})]\text{ClO}_4 \cdot \text{MeOH}$ (**2**ϕ) were obtained by slow evaporation of the filtrate. Found: C 35.54; H 3.68; N 6.70; Cu 7.60; Ni 6.52%. Calcd. for $\text{C}_{25}\text{H}_{31}\text{Br}_2\text{ClCuN}_4\text{NiO}_9$: C 35.37; H 3.68; N 6.60; Cu 7.48; Ni 6.91%.

$[\text{ZnCu}(\text{L}^{2;2})(\text{AcO})]\text{ClO}_4$ (**3**). Reddish brown crystals. Found: C 34.79; H 3.26; N 6.75; Cu 8.07; Zn 7.58%. Calcd. for $\text{C}_{24}\text{H}_{27}\text{Br}_2\text{ClCuN}_4\text{O}_8\text{Zn}$: C 35.00; H 3.30; N 6.80; Cu 7.71; Zn 7.94%. Selected IR [rcm^{-1}] using KBr: 1631, 1592, 1552, 1445, 1293, 1089, 767, 624. m_{ff} per CuZn: 1.85 m_{b} at 290 K. UV-Vis [I_{max}/nm ($\text{e}/\text{M}^{-1} \text{cm}^{-1}$)] in DMSO: 353 (8590), 542 (220).

[CoCu(L^{2:3})(AcO)]ClO₄·0.5H₂O (**4**). Dark green microcrystals. Found: C 35.50; H 3.53; N 6.53; Cu 8.00; Co 6.91%. Calcd. for C₂₅H₃₀Br₂ClCoCuN₄O_{8.5}: C 35.74; H 3.60; N 6.67; Cu 7.56; Co 7.01%. Selected IR [ν/cm^{-1}] using KBr: 1619, 1582, 1456, 1402, 1303, 1094, 690, 622. m_{ff} per CuCo: 4.82 m_{b} at 290 K. UV-Vis [I_{max}/nm ($\text{e}/\text{M}^{-1} \text{cm}^{-1}$)] in DMSO: 356 (8810), 636 (120).

[NiCu(L^{2:3})(AcO)]ClO₄ (**5**). Green crystals. Found: C 36.14; H 3.63; N 6.70; Cu 7.47; Ni 7.00%. Calcd. for C₂₅H₂₉Br₂ClCuNiO₈: C 36.13; H 3.52; N 6.74; Cu 7.65; Ni 7.06%. Selected IR [ν/cm^{-1}] using KBr: 1622, 1609, 1560, 1452, 1302, 1086, 754, 683, 622. m_{ff} per CuNi: 3.36 m_{b} at 290 K. UV-Vis [I_{max}/nm ($\text{e}/\text{M}^{-1} \text{cm}^{-1}$)] in DMSO: 358 (8800), 656 (95).

[ZnCu(L^{2:3})(AcO)]ClO₄·0.5H₂O (**6**). Green microcrystals. Found: C 35.36; H 3.54; N 6.51; Cu 7.91; Zn 7.75%. Calcd. for C₂₅H₃₀Br₂ClCuN₄O_{8.5}Zn: C 35.46; H 3.57; N 6.62; Cu 7.51; Zn 7.72%. Selected IR [ν/cm^{-1}] using KBr: 1620, 1594, 1565, 1453, 1403, 1305, 1085, 776, 689, 623. m_{ff} per CuZn: 1.86 m_{b} at 290 K. UV-Vis [I_{max}/nm ($\text{e}/\text{M}^{-1} \text{cm}^{-1}$)] in DMSO: 352 (8800), 617 (93).

[CoCu(L^{2:4})(AcO(DMF))]ClO₄ (**7**). Recrystallized from DMF as dark brown crystals. Found: C 38.37; H 4.40; N 7.90; Cu 6.92; Co 6.67%. Calcd. for C₂₉H₃₈Br₂ClCoCuN₅O₉: C 37.93; H 4.17; N 7.63; Cu 6.92; Co 6.42%. Selected IR [ν/cm^{-1}] using KBr: 1652, 1622, 1556, 1451, 1450, 1416, 1303, 1097, 1086, 622. m_{ff} per CuCo: 4.99 m_{b} at 290 K. UV-Vis [I_{max}/nm ($\text{e}/\text{M}^{-1} \text{cm}^{-1}$)] in DMSO: 366 (8000), 720 (130).

[NiCu(L^{2:4})(AcO)]ClO₄·2DMF (**8**). Recrystallized from DMF as green microcrystals. Found: C 38.68; H 4.53; N 8.31; Cu 6.16; Ni 5.69%. Calcd. for C₃₂H₄₅Br₂ClCuNiO₁₀: C 38.78; H 4.58; N 8.48; Cu 6.41; Ni 5.92%. Selected IR [ν/cm^{-1}] using KBr: 1674, 1652, 1629, 1565, 1447, 1414, 1302, 1102, 1095, 623. m_{ff} per CuNi: 3.36 m_{b} at 290 K. UV-Vis [I_{max}/nm ($\text{e}/\text{M}^{-1} \text{cm}^{-1}$)] in DMSO: 367 (8700), 720 (150).

[ZnCu(L^{2:4})(AcO)]ClO₄ (**9**). Green crystals. Found: C 36.63; H 3.66; N 6.48; Cu 7.89; Zn 7.66%. Calcd. for C₂₆H₃₁Br₂ClCuN₄O₈Zn: C 36.66; H 3.67; N 6.58; Cu 7.46; Zn 7.68%. Selected IR [ν/cm^{-1}] using KBr: 1618, 1592, 1453, 1402, 1302, 1097, 1090, 622. m_{ff} per CuZn: 1.83 m_{b} at 290 K. UV-Vis [I_{max}/nm ($\text{e}/\text{M}^{-1} \text{cm}^{-1}$)] in DMSO: 355 (8900), 740^{br} (74).

2.1b (Acetato)Cu^{II}M^{II} complexes: To a suspension of a Pb^{II}Cu^{II} precursor [PbCu(L^{m:n})](ClO₄)₂ (1×10^{-4} mol) in acetonitrile (10 cm³) was added a methanol solution (20 cm³) of a M^{II} sulphate salt (1×10^{-4} mol) and sodium acetate (1×10^{-4} mol), and the mixture was stirred at ambient temperature for 3 h to result in the precipitation of PbSO₄. It was removed by filtration and the filtrate was diffused with ether to give a precipitate.

[CuZn(L^{2:3})(AcO)]ClO₄ (**10**)³ was obtained by this method, but other complexes could not be obtained in pure form.

2.2 Physical measurements

Elemental analyses of C, H, and N were obtained at the Service Center of Elemental Analysis, Kyushu University, Japan. Metal analyses were made on a Shimadzu AA-680 atomic absorption/flame emission spectrophotometer. Infrared spectra were recorded on a JASCO IR-810 spectrophotometer using KBr disks. Electronic absorption spectra in dimethyl sulphoxide (DMSO) were recorded on a Shimadzu UV-3100PC spectrophotometer. Reflectance spectra were recorded on a Shimadzu MPS-2000

spectrophotometer. Magnetic susceptibilities of powdered samples were measured on a quantum design MPMS XL SQUID susceptometer over the temperature range of 2–300 K. Diamagnetic corrections for the constituting atoms were made using Pascal's constants⁷. Cyclic voltammograms were measured in DMSO solution containing tetra(*n*-butyl)ammonium perchlorate (TBAP) as the supporting electrolyte, using a BAS CV-50 W electrochemical analyser (**Caution!** TBAP is explosive and should be handled with great care). A three-electrode cell was used which was equipped with a glassy carbon working electrode, a platinum coil as the counter electrode, and a Ag/Ag⁺ (TBAP/acetonitrile) reference electrode.

2.3 X-ray crystallography

Each single crystal of [NiCu(L^{2:2})(AcO)]ClO₄·MeOH (**2**'), [ZnCu(L^{2:2})(AcO)]ClO₄ (**3**), [NiCu(L^{2:3})(AcO)]ClO₄ (**5**), [CoCu(L^{2:4})(AcO)(DMF)]ClO₄ (**7**) and [ZnCu(L^{2:4})(AcO)]ClO₄ (**9**) was mounted on a glass fibre and coated with epoxy resin. All the crystallographic measurements were performed on a Rigaku AFC7R diffractometer with graphite monochromated Mo-K α radiation ($\lambda = 0.71069 \text{ \AA}$) and a 12 kW rotating anode generator at $20 \pm 1 \text{ }^\circ\text{C}$. Cell constants and an orientation matrix for the data collection were obtained from 25 reflections in the range $29.84 < 2\theta < 29.97^\circ$ for **2**', 25 reflections in the range $29.67 < 2\theta < 29.99^\circ$ for **3**, 24 reflections in the range $26.87 < 2\theta < 30.01^\circ$ for **5**, 22 reflections in the range $29.59 < 2\theta < 30.04^\circ$ for **7**, and 20 reflections in the range $6.30 < 2\theta < 10.59^\circ$ for **9**. For the intensity collections, the $\omega - 2\theta$ scan mode was used to a maximum 2θ value of 55.0° for all the complexes at a scan speed of $16.0^\circ/\text{min}$ (in omega). The octant measured was +h, +k, \pm l for all the complexes. Pertinent crystallographic parameters are summarized in table 1.

Three standard reflections were monitored for every 150 measurements. Over the course of the data collection, the standards decreased by 0.7% for **2**', 11.8% for **3**, 0.7% for **5**, 8.2% for **7** and 6.6% for **9**. A linear correction factor was applied to the data to account for the phenomena. An empirical absorption correction based on azimuthal scans of several reflections was applied which resulted in transmission factors ranging from 0.58 to 1.00 for **2**', from 0.61 to 1.00 for **3**, from 0.89 to 1.00 for **5**, from 0.61 to 1.00 for **7** and from 0.70 to 1.00 for **9**. Reflection data were corrected for Lorentz and polarization effects.

The structures were solved by the direct method and expanded using Fourier techniques. The non-hydrogen atoms were refined anisotropically except for the case of **7**. The perchlorate ion in **7** was positioned at a special equivalent position in the crystal lattice (occupancy factor 0.5) and its oxygens were disordered. The refinement of **7** was performed by assuming the perchlorate ion as a rigid ball. Hydrogen atoms were included in the structure factor calculation but were not refined. Neutral atom scattering factors were taken from Cromer and Waber⁸. Anomalous dispersion effects were included in the final calculations⁹; the values for $\Delta f'$ and $\Delta f''$ were taken from reference [10] and those for the mass-attenuation coefficients from reference [11]. Computations were carried out on an IRIS Indigo computer using the TEXSAN crystallographic software package of the Molecular Structure Corporation¹².

Table 1. Crystallographic data of [NiCu(L)^{2,2'}(AcO)]ClO₄·MeOH (**2'**), [ZnCu(L)^{2,2'}(AcO)]ClO₄ (**3**), [NiCu(L)^{2,2'}(AcO)]ClO₄ (**5**), [CoCu(L^{2,2'}(AcO)(dmf)]ClO₄ (**7**) and [ZnCu(L^{2,2'}(AcO)]ClO₄ (**9**).

Complex	2c	3	5	7	9
Complex formula	C ₂₅ H ₃₁ Br ₂ ClCuN ₄ NiO ₉	C ₂₄ H ₂₇ Br ₂ ClCuN ₄ O ₈ Zn	C ₂₅ H ₂₉ Br ₂ ClCuN ₄ NiO ₉	C ₂₉ H ₃₈ Br ₂ ClCoCuN ₅ O ₉	C ₂₆ H ₃₁ Br ₂ ClCuN ₄ O ₈ Zn
f.w.	849.05	823.69	831.03	918.39	851.74
Crystal colour	Dark green	Purple brown	Green	Brown	Green
Crystal size/mm ³	0.40 × 0.25 × 0.20	0.60 × 0.60 × 0.60	0.30 × 0.30 × 0.18	0.25 × 0.25 × 0.25	0.30 × 0.30 × 0.25
Crystal system	Triclinic	Triclinic	Monoclinic	Triclinic	Monoclinic
Space group	P1 (#1)	P1 (#2)	P2 _{1/c} (#14)	P1 (#2)	P2 _{1/c} (#14)
a/Å	7.962	11.526(2)	9.301(4)	10.390(9)	9.658(2)
b/Å	13.797(3)	14.815(3)	18.83(1)	20.32(1)	19.459(5)
c/Å	15.060(4)	9.039(2)	17.274(3)	9.496(8)	17.225(7)
a/deg	109.23(2)	97.98(2)	98.55(3)	102.48(6)	97.84(2)
b/deg	105.69(2)	104.23(2)	2992(1)	107.26(6)	3206(1)
g/deg	89.60(2)	77.03(1)	4	81.18(6)	4
V/Å ³	1497(1)	1452.3(5)	2	1860(2)	4
Z	2	2	4	2	4
D _{calcd} /g cm ⁻³	1.882	1.883	1.844	1.639	1.764
m(Mo-Kα)/cm ⁻¹	41.62	44.63	41.61	32.98	40.46
No. of reflections (I > 3.00 σ(I))	5144	4805	3884	4877	4079
F(000)	850	818	1660	924	1700
R ^a	0.052	0.072	0.039	0.101	0.068
R _w ^{b,c}	0.040	0.097	0.025	0.115	0.077

^aR = $\sum ||F_o| - |F_c|| / \sum |F_o|$, ^bR_w = $[\sum w(|F_o| - |F_c|)^2 / \sum w|F_o|^2]^{1/2}$, ^cw = 1/σ(|F_o|)²

3. Results and discussion

3.1 Synthesis

A series of the (acetato) $\text{M}^{\text{II}}\text{Cu}^{\text{II}}$ complexes, $[\text{MCu}(\text{L}^{\text{m:n}})(\text{AcO})]\text{ClO}_4$ ($(\text{L}^{\text{m:n}})^{2-} = (\text{L}^{2:2})^{2-} \sim (\text{L}^{2:4})^{2-}$; **1** ~ **9**), were obtained when the mononuclear Cu^{II} precursors $[\text{Cu}(\text{L}^{2:2})] \sim [\text{Cu}(\text{L}^{2:2})]$ were treated with a M^{II} perchlorate salt and a M^{II} acetate salt in methanol at the refluxing temperature (method **I**). In our attempt to prepare the (acetato) $\text{Cu}^{\text{II}}\text{M}^{\text{II}}$ complexes by method **II**, on the other hand, only $[\text{CuZn}(\text{L}^{2:3})(\text{AcO})]\text{ClO}_4$ (**10**) could be obtained in a pure form. In other cases, the resulting products contained a large copper content relative to the M content. FAB mass spectrometric studies indicated the presence of $[\text{CuCu}(\text{L}^{\text{m:n}})(\text{AcO})]^+$ as the main species along with a small amount of $[\text{CuM}(\text{L}^{\text{m:n}})(\text{AcO})]^+$. It appears that the (acetato) $\text{Cu}^{\text{II}}\text{M}^{\text{II}}$ complexes, except for **10**, are thermodynamically unstable to cause a scrambling of metal ions.

3.2 Crystal structures

X-ray crystallographic studies were carried out for **2** ζ **3**, **5**, **7** and **9** to see the site selectivity of metal ions and their core structures.

$[\text{NiCu}(\text{L}^{2:2})(\text{AcO})]\text{ClO}_4 \cdot \text{MeOH}$ (**2'**). An ORTEP¹³ view of the cationic part of **2'** is shown in figure 1 together with the numbering scheme. Selected bond distances and angles are summarized in table 2.

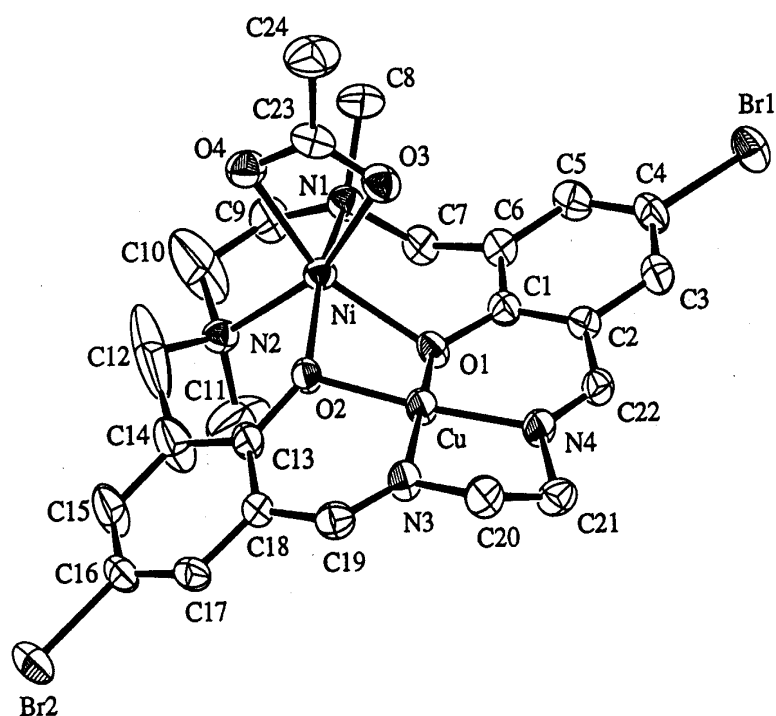


Figure 1. An ORTEP view of $[\text{NiCu}(\text{L}^{2:2})(\text{AcO})]\text{ClO}_4 \cdot \text{MeOH}$ (**2'**) with the atom numbering scheme.

Table 2. Selected bond distances and angles for [NiCu(L^{2:2})(AcO)]ClO₄·MeOH (**2**’).

<i>Bond distances (Å)</i>			
Ni–O(1)	2.119(4)	Cu–O(1)	1.908(4)
Ni–O(2)	2.071(4)	Cu–O(2)	1.890(4)
Ni–O(3)	2.069(4)	Cu–N(3)	1.921(4)
Ni–O(4)	2.120(4)	Cu–N(4)	1.898(4)
Ni–N(1)	2.101(4)	Ni...Cu	2.972(1)
Ni–N(2)	2.058(5)		
<i>Bond angles (deg)</i>			
Ni–O(1)–Cu	95.0(1)	O(3)–Ni–N(1)	98.8(2)
Ni–O(2)–Cu	97.1(1)	O(3)–Ni–N(2)	158.3(2)
O(1)–Ni–O(2)	76.2(1)	O(4)–Ni–N(1)	98.2(2)
O(1)–Ni–O(3)	88.2(2)	O(4)–Ni–N(2)	95.7(2)
O(1)–Ni–O(4)	150.4(2)	N(1)–Ni–N(2)	86.2(2)
O(1)–Ni–N(1)	91.5(2)	O(1)–Cu–O(2)	85.8(2)
O(1)–Ni–N(2)	112.9(2)	O(1)–Cu–N(3)	171.4(2)
O(2)–Ni–O(3)	92.5(2)	O(1)–Cu–N(4)	96.0(2)
O(2)–Ni–O(4)	98.2(1)	O(2)–Cu–N(3)	92.8(2)
O(2)–Ni–N(1)	163.1(2)	O(2)–Cu–N(4)	174.0(2)
O(2)–Ni–N(2)	88.0(2)	N(3)–Cu–N(4)	86.2(2)
O(3)–Ni–O(4)	62.8(2)		
<i>Dihedral angles (deg)</i>			
O(1)O(2)N(1)N(2)–O(1)O(2)N(3)N(4)11.96			

The cation has a heterodinuclear core with the Ni^{II} in the aminic site and the Cu^{II} in the iminic site with the Ni–Cu intermetallic separation of 2.972(1) Å. The acetate group coordinates to the Ni^{II} as a chelating ligand to provide a distorted six-coordinate geometry about the metal; the methanol molecule is free from coordination and is captured in the crystal lattice. The Ni-to-donor bond distances range from 2.058(5) to 2.120(4) Å. The Ni is displaced by 0.721 Å from the basal N(amine)₂O₂ least-squares plane toward the acetate ion. The geometry around the Cu^{II} is essentially planar with the Cu-to-donor bond distances ranging from 1.890(4) to 1.921(4) Å. The Ni–O1–Cu and Ni–O2–Cu angles are 95.0(1)° and 97.1° respectively. The N(amine)₂O₂ least-squares plane and the N(imine)₂O₂ least-squares plane are bent at the O1–O2 edge with a dihedral angle of 11.96°.

The asymmetric nitrogens N1 and N2 have the same confirmation (*S* and *S*), and the two methyl groups attached to the nitrogens are situated *trans* to each other and axially oriented with respect to the mean N(amine)₂O₂ plane. In the M^{II}Cu^{II} complexes of (L^{2:2})²⁻ and (L^{2:3})²⁻ so far characterized, the M^{II} assumes a five-coordinate geometry where the aminic nitrogens have different configurations (*R* and *S*) with the *cis* arrangement of the two methyl groups with respect to the en-chelate²⁻⁴.

[ZnCu(L^{2:2})(AcO)]ClO₄ (**3**). An ORTEP drawing of the cationic part of **3** is shown in figure 2 together with the numbering scheme. Selected bond distances and angles are given in table 3.

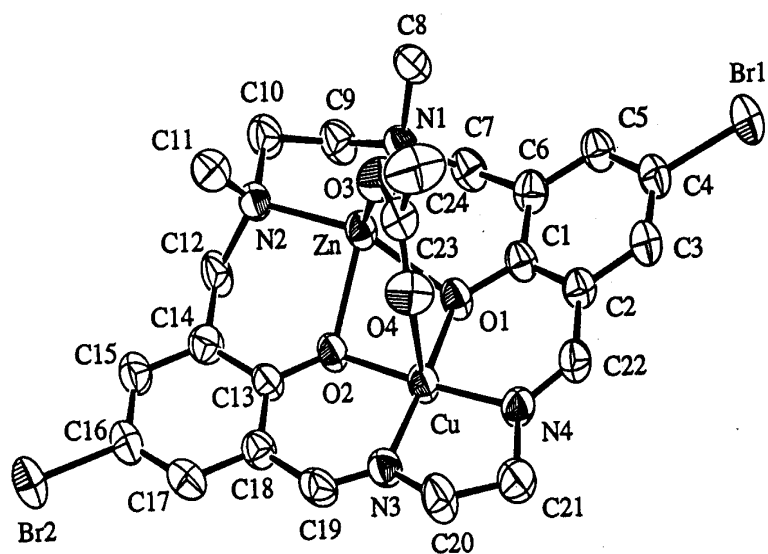


Figure 2. An ORTEP view of $[ZnCu(L^{2,2})(AcO)]ClO_4$ (**3**) with the atom numbering scheme.

Table 3. Selected bond distances and angles for $[ZnCu(L^{2,2})(AcO)]ClO_4$ (**3**).

Bond distances (Å)

Zn–O(1)	2.122(5)	Cu–O(2)	1.904(4)
Zn–O(2)	2.078(4)	Cu–O(4)	2.493(5)
Zn–O(3)	1.924(5)	Cu–N(3)	1.900(6)
Zn–N(1)	2.094(5)	Cu–N(4)	1.911(6)
Zn–N(2)	2.088(6)	Zn...Cu	2.872(1)
Cu–O(1)	1.894(4)		

Bond angles (deg)

Zn–O(1)–Cu	91.1(2)	N(1)–Zn–N(2)	89.1(2)
Zn–O(2)–Cu	92.2(2)	O(1)–Cu–O(2)	81.1(2)
O(1)–Zn–O(2)	72.1(2)	O(1)–Cu–O(4)	94.4(2)
O(1)–Zn–O(3)	104.8(2)	O(1)–Cu–N(3)	175.8(2)
O(1)–Zn–N(1)	87.6(2)	O(1)–Cu–N(4)	95.4(2)
O(1)–Zn–N(2)	147.4(2)	O(2)–Cu–O(4)	93.6(2)
O(2)–Zn–O(3)	117.3(2)	O(2)–Cu–N(3)	95.2(2)
O(2)–Zn–N(1)	137.8(2)	O(2)–Cu–N(4)	176.4(2)
O(2)–Zn–N(2)	89.2(2)	O(4)–Cu–N(3)	87.9(2)
O(3)–Zn–N(1)	103.3(2)	O(4)–Cu–N(4)	85.4(2)
O(3)–Zn–N(2)	107.6(2)	N(3)–Cu–N(4)	88.2(2)

Dihedral angles (deg)

O(1)O(2)N(1)N(2)–O(1)O(2)N(3)N(4)24.93

The cation has a dinuclear core with the Zn^{II} in the aminic site and the Cu^{II} in the iminic site. The acetate ion bridges the Zn^{II} and Cu^{II} ions to afford a five-coordinate environment for the two metal ions. The Zn–Cu intermetallic separation is 2.872(1) Å. The geometry about the Zn can be regarded as a distorted square-pyramid with the N_2O_2 donor atoms on the base and the acetate oxygen at the apex. The geometric discrimination factor t^{14} between square-pyramid ($t = 0$) and trigonal-bipyramid ($t = 1$) is 0.16. The Zn is displaced by 0.66 Å from the basal least-squares plane toward the acetate oxygen. The basal Zn–N and Zn–O bond distances range from 2.078(4) to 2.122(5) Å. The axial Zn–O3 (acetate) bond distance is shorter (1.924(5) Å). The geometry about the Cu^{II} is also square-pyramidal ($t = 0.01$). The basal Cu–N and Cu–O bond distances (1.894(4) ~ 1.911(6) Å) are significantly short, relative to the basal Zn–N and Zn–O bond distances. The axial Cu–O4 (acetate) bond is elongated (2.493(5) Å) owing to the Jahn-Teller effect for d^9 electronic configuration. The Cu is displaced by 0.007 Å from the basal least-squares plane toward O4. The $\text{N}(\text{amine})_2\text{O}_2$ and the $\text{N}(\text{imine})_2\text{O}_2$ least-squares planes are bent at the O1–O2 edge with a dihedral angle of 24.93°. The asymmetric nitrogens N1 and N2 have different configurations (*S* and *R*); the two methyl substituents on the aminic nitrogens are situated *cis* to each other and are axially oriented with respect to the mean $\text{N}(\text{amine})_2\text{O}_2$ plane.

$[\text{NiCu}(\text{L}^{2,3})(\text{AcO})]\text{ClO}_4$ (**5**). An ORTEP drawing of the cationic part of **5** is shown in figure 3 together with the numbering scheme. Selected bond distances and angles are given in table 4.

The X-ray crystallography demonstrates a dinuclear core with the Ni^{II} in the aminic site and the Cu^{II} in the iminic site. The acetate group bridges the two metal ions in the Ni–Cu intermetallic separation of 2.935(1) Å. The geometry about the Ni can be regarded

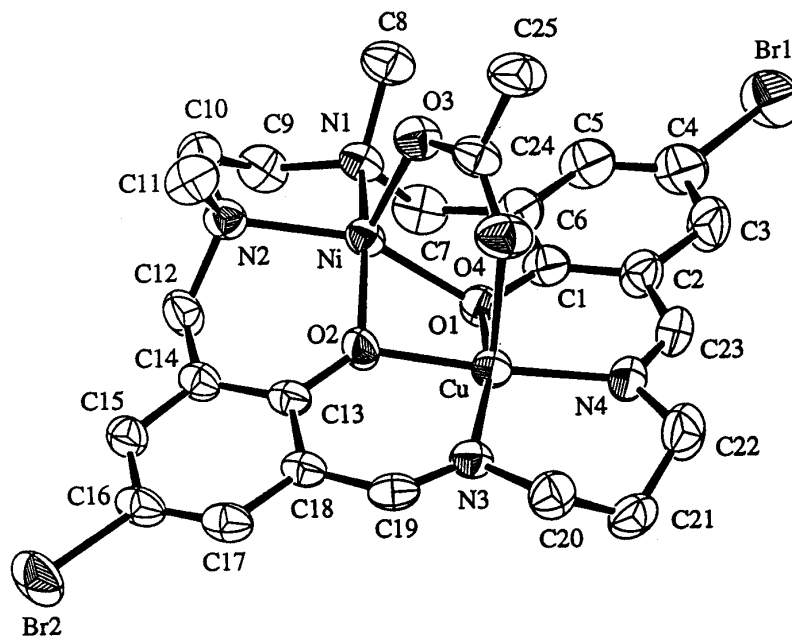


Figure 3. An ORTEP view of $[\text{NiCu}(\text{L}^{2,3})(\text{AcO})]\text{ClO}_4$ (**5**) with the atom numbering scheme.

Table 4. Selected bond distances and angles for $[\text{NiCu}(\text{L}^{2,3})(\text{AcO})]\text{ClO}_4$ (**5**).

<i>Bond distances (Å)</i>			
Ni–O(1)	2.009(3)	Cu–O(2)	1.936(3)
Ni–O(2)	1.963(3)	Cu–O(4)	2.205(4)
Ni–O(3)	1.962(3)	Cu–N(3)	1.972(4)
Ni–N(1)	2.049(4)	Cu–N(4)	1.971(4)
Ni–N(2)	2.054(4)	Ni...Cu	2.935(1)
Cu–O(1)	1.978(3)		
<i>Bond angles (deg)</i>			
Ni–O(1)–Cu	94.8(1)	N(1)–Ni–N(2)	88.4(2)
Ni–O(2)–Cu	97.7(1)	O(1)–Cu–O(2)	77.6(1)
O(1)–Ni–O(2)	76.3(1)	O(1)–Cu–O(4)	92.6(1)
O(1)–Ni–O(3)	99.8(1)	O(1)–Cu–N(3)	160.1(1)
O(1)–Ni–N(1)	94.3(1)	O(1)–Cu–N(4)	90.3(2)
O(1)–Ni–N(2)	155.5(1)	O(2)–Cu–O(4)	88.5(1)
O(2)–Ni–O(3)	105.3(1)	O(2)–Cu–N(3)	90.3(2)
O(2)–Ni–N(1)	156.3(2)	O(2)–Cu–N(4)	169.2(2)
O(2)–Ni–N(2)	91.7(1)	O(4)–Cu–N(3)	102.9(1)
O(3)–Ni–N(1)	97.7(1)	O(4)–Cu–N(4)	93.1(2)
O(3)–Ni–N(2)	104.0(2)	N(3)–Cu–N(4)	99.8(2)
<i>Dihedral angles (deg)</i>			
O(1)O(2)N(1)N(2)–O(1)O(2)N(3)N(4)15.77			

as a square-pyramid with the acetate oxygen (O3) at the apex (t : 0.152). The basal Ni–N and Ni–O bond distances fall in the range of 1.963(3) ~ 2.054(4) Å. The axial Ni–O3 bond is shorter (1.962(3) Å). The Ni is displaced by 0.407 Å from the basal least-squares plane towards the axial site. The geometry about the Cu is square-pyramidal with the acetate oxygen O4 at the apex (t : 0.013). The basal Cu–N and Cu–O bond distances range from 1.936(3) to 1.978(3) Å. The axial Cu–O4 bond distance is elongated (2.205(4) Å). The displacement of the Cu from the basal N_2O_2 least-squares plane toward O4 is 0.170 Å. The bending between the $\text{N}(\text{amine})_2\text{O}_2$ and $\text{N}(\text{imine})_2\text{O}_2$ least-squares planes at the O1–O2 edge is 15.77°. The asymmetric nitrogens N1 and N2 have different configurations (*S* and *R*); the two methyl substituents on the aminic nitrogens are situated *cis* to each other and are axially oriented with respect to the mean $\text{N}(\text{amine})_2\text{O}_2$ plane.

$[\text{CoCu}(\text{L}^{2,4})(\text{AcO})(\text{DMF})]\text{ClO}_4$ (**7**). An ORTEP drawing of the cationic part of **7** is shown in figure 4. Selected bond distances and angles are given in table 5.

The dinuclear core has the Co^{II} in the aminic site and the Cu^{II} in the iminic site and the acetate group bridges the metal ions in the Co–Cu separation of 3.023(3) Å. The O1–N1–N2–O2 entity assumes a non-planar configuration providing a *cis*-b octahedral geometry about the Co with the acetate oxygen O3 and the DMF oxygen O5 in *cis* positions. The Co–N and Co–O bond distances range from 2.005(8) to 2.17(1) Å.

The Cu^{II} assumes a distorted trigonal-bipyramidal geometry with O1 and N3 of the macrocycle at the axial sites and with O2 and N4 of the macrocycle and the O4 of the bridging acetate group on the equatorial base. The axial Cu–O1 and Cu–N3 bond distances are 1.929(9) and 1.97(1) Å respectively and the O1–Cu–N3 angle is 169.1(5)°. The equatorial Cu–O2, Cu–N4 and Cu–O4 bond distances are longer (2.11(1), 1.98(1)

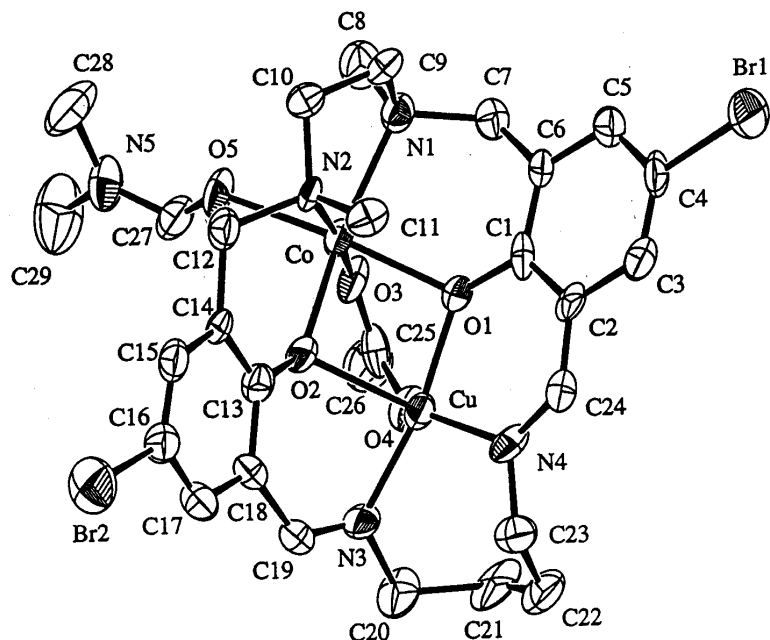


Figure 4. An ORTEP view of $[\text{CoCu}(\text{L}^{2+})(\text{AcO})(\text{DMF})]\text{ClO}_4$ (**7**) with the atom numbering scheme.

Table 5. Selected bond distances and angles for $[\text{CoCu}(\text{L}^{2+})(\text{AcO})(\text{DMF})]\text{ClO}_4$ (**7**).

Bond distances (\AA)			
Co–O(1)	2.117(9)	Cu–O(1)	1.929(9)
Co–O(2)	2.005(8)	Cu–O(2)	2.11(1)
Co–O(3)	2.06(1)	Cu–O(4)	2.06(1)
Co–O(5)	2.106(9)	Cu–N(3)	1.97(1)
Co–N(1)	2.14(1)	Cu–N(4)	1.98(1)
Co–N(2)	2.17(1)	Co...Cu	3.023(3)
Bond angles (deg)			
Co–O(1)–Cu	96.6(3)	O(5)–Co–N(1)	94.9(4)
Co–O(2)–Cu	94.6(4)	O(5)–Co–N(2)	87.6(4)
O(1)–Co–O(2)	80.6(4)	N(1)–Co–N(2)	81.0(4)
O(1)–Co–O(3)	85.4(4)	O(1)–Cu–O(2)	82.6(4)
O(1)–Co–O(5)	171.9(4)	O(1)–Cu–O(4)	90.5(4)
O(1)–Co–N(1)	88.9(4)	O(1)–Cu–N(3)	169.1(5)
O(1)–Co–N(2)	100.1(4)	O(1)–Cu–N(4)	91.8(4)
O(2)–Co–O(3)	93.3(4)	O(2)–Cu–O(4)	93.6(4)
O(2)–Co–O(5)	97.6(4)	O(2)–Cu–N(3)	86.7(5)
O(2)–Co–N(1)	161.2(4)	O(2)–Cu–N(4)	130.9(5)
O(2)–Co–N(2)	85.6(4)	O(4)–Cu–N(3)	91.6(4)
O(3)–Co–O(5)	86.8(4)	O(4)–Cu–N(4)	135.4(5)
O(3)–Co–N(1)	101.4(4)	N(3)–Cu–N(4)	94.2(4)
O(3)–Co–N(2)	174.2(4)		
Dihedral angles (deg)			
O(1)O(2)N(1)N(2)–O(1)O(2)N(3)N(4)41.37			

and 2.06 Å, respectively). The equatorial plane shows a large distortion from the triangle; the O2–Cu–N4, O2–Cu–O4 and N4–Cu–O4 angles are 130.9(5), 93.6(4) and 135.4(5)° respectively. The bridging phenolic oxygen O2 shows a distortion to tetrahedron as seen in the sum of the angles of Co–O2–Cu, Co–O2–C13 and Cu–O2–C13 (345.2°). The asymmetric amino nitrogens N1 and N2 have the same configuration (*R*), and the two methyl groups attached to the nitrogens are situated *trans* with respect to the enchelate ring.

[ZnCu(L^{2:4})(AcO)]ClO₄ (**9**). An ORTEP drawing of the cationic part of **9** is shown in figure 5 together with the numbering scheme. Selected bond distances and angles are given in table 6.

The dinuclear core has the Zn^{II} in the aminic site and the Cu^{II} in the iminic site. The acetate group bridges the two metal ions in the Cu–Zn intermetallic separation of 2.980(2) Å. The geometry about the Zn is square-pyramidal with the N₂O₂ donor atoms on the base and the acetate oxygen O3 at the apex (*t*: 0.14). The axial Zn–O3 bond distance (1.912(6) Å) is short, relative to the basal bond distances (2.107(7)–2.086(5) Å). The displacement of the Zn from the basal least-squares plane is 0.621 Å. The geometry about the Cu in the iminic site is also square-pyramidal with an acetate oxygen O4 at the apex (*t*: 0.03). The basal bond distances fall in the range of 1.937(5)–2.004(7) Å. The axial Cu–O4 bond distance is elongated (2.270(7) Å). The Cu is

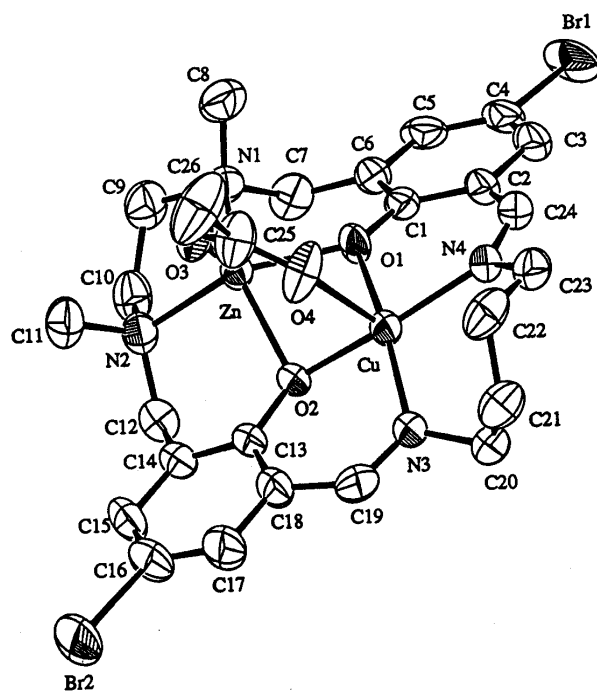


Figure 5. An ORTEP view of [ZnCu(L^{2:4})(AcO)]ClO₄ (**9**) with the atom numbering scheme.

Table 6. Selected bond distances and angles for [ZnCu(L^{2:4})(AcO)]ClO₄ (**9**).

<i>Bond distances (Å)</i>			
Zn–O(1)	2.031(5)	Cu–O(2)	1.978(5)
Zn–O(2)	2.086(5)	Cu–O(4)	2.270(7)
Zn–O(3)	1.912(6)	Cu–N(3)	1.953(7)
Zn–N(1)	2.107(7)	Cu–N(4)	2.004(7)
Zn–N(2)	2.107(7)	Zn...Cu	2.980(2)
Cu–O(1)	1.937(5)		
<i>Bond angles (deg)</i>			
Zn–O(1)–Cu	97.3(2)	N(1)–Zn–N(2)	86.0(3)
Zn–O(2)–Cu	94.3(2)	O(1)–Cu–O(2)	79.0(2)
O(1)–Zn–O(2)	74.4(2)	O(1)–Cu–O(4)	88.0(2)
O(1)–Zn–O(3)	105.3(3)	O(1)–Cu–N(3)	166.6(3)
O(1)–Zn–N(1)	88.3(2)	O(1)–Cu–N(4)	89.0(3)
O(1)–Zn–N(2)	149.1(3)	O(2)–Cu–O(4)	90.0(2)
O(2)–Zn–O(3)	105.3(2)	O(2)–Cu–N(3)	90.2(3)
O(2)–Zn–N(1)	140.5(3)	O(2)–Cu–N(4)	164.8(3)
O(2)–Zn–N(2)	91.1(2)	O(4)–Cu–N(3)	99.9(3)
O(3)–Zn–N(1)	113.5(3)	O(4)–Cu–N(4)	98.8(3)
O(3)–Zn–N(2)	104.8(3)	N(3)–Cu–N(4)	100.3(3)
<i>Dihedral angles (deg)</i>			
O(1)O(2)N(1)N(2)–O(1)O(2)N(3)N(4)10.00			

displaced by 0.163 Å from the basal least-squares plane toward O4. The N(amine)₂O₂ and the N(imine)₂O₂ least-squares planes are bent at the O1–O2 edge with a dihedral angle of 10.0°. The asymmetric amino nitrogens N1 and N2 have different configurations (*S* and *R*), and the two methyl substituents on the aminic nitrogens are situated *cis* to each other and are axially oriented with respect to the mean N(amine)₂O₂ plane.

[CuZn(L^{2:3})(AcO)]ClO₄ (**10**). The crystal structure of this complex was previously determined³. It has the Cu^{II} in the aminic site and the Zn^{II} in the iminic site, bridged by an acetate group in the syn:syn mode. The result demonstrates the migration of the Cu^{II} from the iminic site to aminic site in the transmetallation process. The assignment of the positions of the metal ions is based on the relative metal–N and M–O bond distances and the geometric features of the two chromophores. The {CuN(amine)₂O₂} site assumes a square-pyramidal geometry. The basal Cu–N and Cu–O bond distances range from 1.973(6) to 2.026(8) Å, and the axial Cu–O(acetate) bond (2.093(7) Å) is slightly elongated owing to the Jahn-Teller effect. The {ZnN(imine)₂O₂} site also assumes a square-pyramidal geometry. The basal Zn–N and Zn–O bond distances (2.029(8)–2.061(6) Å) are longer than the corresponding bond distances of {CuN(amine)₂O₂}. Instead, the axial Zn–O(acetate) distance is short (2.018(6) Å).

3.3 Kinetic and thermodynamic macrocyclic effect

From the above crystallographic studies, it is evident that (L^{2:2})²⁻, (L^{2:3})²⁻ and (L^{2:4})²⁻ show a site selectivity of metal ions, providing the (acetato)M^{II}Cu^{II} complexes (M = Co, Ni, Zn). The acetate group acts as a bidentate chelating ligand to the M^{II} or a bridging ligand between the Cu^{II} and M^{II} ions. In both the chelating and bridging functions, the acetate group probably plays an important role in stabilizing the M^{II}Cu^{II} core.

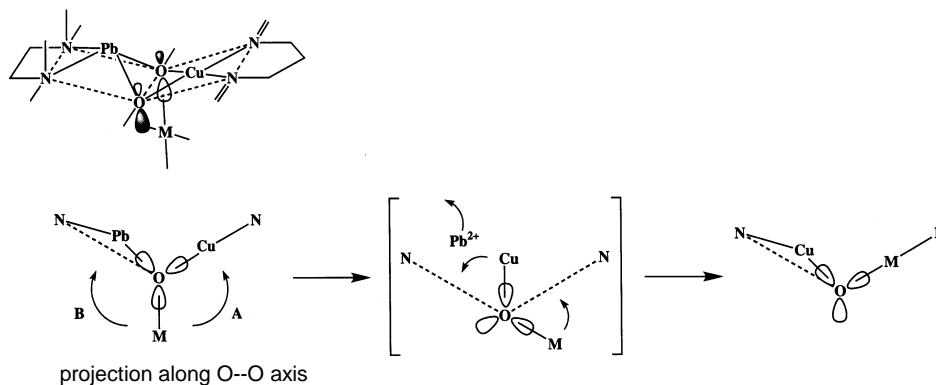
It is interesting to see the core structures of the complexes with respect to the M^{II} in the aminic site and the ring size of the macrocyclic ligands. In the $\text{Ni}^{\text{II}}\text{Cu}^{\text{II}}$ complex **2** of $(\text{L}^{2:2})^{2-}$, the Ni^{II} cannot reside within the aminic cavity and is largely displaced from the $\text{N}(\text{amine})_2\text{O}_2$ least-squares plane (0.721 Å). The bidentate chelation of the acetate ion to the Ni^{II} is preferred in this case. In the $\text{Zn}^{\text{II}}\text{Cu}^{\text{II}}$ complex **3** of $(\text{L}^{2:2})^{2-}$, the acetate-bridged core is formed because the Zn displacement from the $\text{N}(\text{amine})_2\text{O}_2$ least-squares plane is smaller (0.66 Å) and Zn^{II} prefers five-coordination to six-coordination. In the $\text{Ni}^{\text{II}}\text{Cu}^{\text{II}}$ complex **5** of $(\text{L}^{2:3})^{2-}$, the elongation of the lateral chain in the iminic site gives rise to a considerable adaptability for the aminic site to accommodate the Ni^{II} ion. The displacement of the Ni in this complex is small (0.407 Å) so that the acetate-bridged core is preferred. The macrocycle $(\text{L}^{2:4})^{2-}$ has a higher adaptability for complexation due to further elongation in the lateral chain in the iminic site. In the $\text{Co}^{\text{II}}\text{Cu}^{\text{II}}$ complex **7**, the N_2O_2 donor atoms in the aminic site are arranged in a non-polar manner, providing a *cis-b* six-coordination about the Co^{II} with an acetate oxygen and a DMF oxygen in *cis* positions. This accompanies a significant distortion about the Cu^{II} in the iminic site as previously discussed.

Of particular interest is the Cu migration in the transmetallation to convert $[\text{PbCu}(\text{L}^{2:3})](\text{ClO}_4)_2$ into $[\text{CuM}(\text{L}^{2:3})(\text{AcO})]\text{ClO}_4$. Previously, this site-selectivity for metal ions was explained by the relative sizes of the metal ions and the metal-binding cavities (thermodynamic macrocyclic effect)³. However, the present study strongly suggests that the formation of $[\text{CuM}(\text{L}^{2:3})(\text{AcO})]\text{ClO}_4$ is kinetically controlled and is known as the kinetic macrocyclic effect. A mechanistic scheme for the Cu migration is discussed here.

A mechanism involving the dissociation of Pb^{II} prior to the attack of M^{II} is ruled out because this may provide the $(\text{acetato})\text{M}^{\text{II}}\text{Cu}^{\text{II}}$ form. Instead, the transmetallation may occur through an association mechanism. Based on the X-ray structure analysis for a $\text{Pb}^{\text{II}}\text{Cu}^{\text{II}}$ complex of $(\text{L}^{2:3})^{2-3}$ the aminic and iminic least-squares planes are bent at the O–O edge with a dihedral angle of 14.87°. This means that the bridging phenolic oxygens have sp^3 hybridization character. Thus, the $\text{Pb}^{\text{II}}\text{Cu}^{\text{II}}$ complex can bind an M^{II} ion through the phenolic oxygens to form a $\text{di}(\text{m}^3\text{-phenoxo})\text{Pb}^{\text{II}}\text{Cu}^{\text{II}}\text{M}^{\text{II}}$ complex (scheme 2). Two paths are considered for the transmetallation. Path **A** is a concerted mechanism involving the approach of the M to the iminic site, the migration of the Cu to the aminic site and the release of the Pb from the aminic site. This can be performed without the cleavage of the O–Cu and O–M bonds, by rotating the O–Cu and O–M linkages with respect to the O–O axis (see scheme 2). When the M approaches the aminic site to eject the Pb (path **B**), the $\text{M}^{\text{II}}\text{Cu}^{\text{II}}$ core may be formed. This is not the case with the transmetallation observed. In fact, path **B** can be ruled out because the $\{\text{MN}(\text{amine})_2\text{O}_2\}$ entity assumes, at least transiently, an energetically unfavourable configuration with a Cu displacement toward the ethylene chain side. It must be noted that in all the $\text{M}^{\text{II}}\text{Cu}^{\text{II}}$ complexes so far characterized, the $\{\text{MN}(\text{amine})_2\text{O}_2\}$ entity has the M displacement toward the N-methyl substituent side. Thus, path **A** can explain the result observed. Such a Cu migration probably occurs in other transmetallations of $[\text{PbCu}(\text{L}^{\text{m:n}})](\text{ClO}_4)_2$ to form $(\text{acetato})\text{Cu}^{\text{II}}\text{M}^{\text{II}}$ complexes. The latter are however thermodynamically unstable and are not isolated.

3.4 Physicochemical properties

3.4a *Infrared spectra*: All the complexes show the $\nu(\text{C}=\text{N})$ vibration of azomethine group at 1632 ~ 1618 cm^{-1} . Complex **2** shows the $\nu_{\text{as}}(\text{COO})$ and $\nu_{\text{s}}(\text{COO})$ vibrations of



Scheme 2. Mechanistic schemes for the Cu migration in the transmetallation reaction.

the acetate group at 1583 and 1445 cm^{-1} respectively. The separation between the two vibrations is smaller than 200 cm^{-1} , in accord with the chelating mode of the acetate group¹⁵. Similarly, the separation between the $\nu_{\text{as}}(\text{COO})$ and $\nu_{\text{s}}(\text{COO})$ vibrations for the other complexes is less than 200 cm^{-1} , in agreement with the bridging function of the acetate group proved for **3**, **5**, **7** and **9**. The ν_{s} mode of the perchlorate group at 1100 ~ 1080 cm^{-1} shows no appreciable splitting. Complex **7** shows an intense band at 1652 cm^{-1} that can be attributed to the $\nu(\text{C}=\text{O})$ vibration of the coordinated DMF molecule. Complex **8** has two IR bands at 1674 and 1652 cm^{-1} attributable to the $\nu(\text{C}=\text{O})$ modes of DMF.

It must be emphasized that isomeric $[\text{ZnCu}(\text{L}^{2:3})(\text{AcO})]\text{ClO}_4$ (**6**) and $[\text{CuZn}(\text{L}^{2:3})(\text{AcO})]\text{ClO}_4$ (**10**) are differentiated by IR spectra. For example, the former shows the $\nu_{\text{as}}(\text{COO})$ and $\nu_{\text{s}}(\text{COO})$ vibrations at 1594 and 1453 cm^{-1} respectively, whereas the latter shows the corresponding vibrations at 1575 and 1450 cm^{-1} respectively.

3.4b Electronic spectra: Absorption spectra of **1** ~ **9** in DMSO are characterized by an intense absorption in the near ultraviolet region and a weak broad absorption in the visible region. The former band at 352 ~ 367 nm is assigned to the intraligand $\text{p} - \text{p}^*$ band associated with the azomethine linkage^{16,17} and the latter band to a superposition of Cu^{II} $d-d$ transition bands. The superposed $d-d$ band is located at 542 ~ 555 nm for **1** ~ **3** of $(\text{L}^{2:2})^{2-}$, at 617 ~ 656 nm for **4** ~ **6** of $(\text{L}^{2:3})^{2-}$, and at 720 ~ 740 nm for **7** ~ **9** of $(\text{L}^{2:4})^{2-}$. This is in accord with the decreasing ligand field strength of the $\{\text{CuN}(\text{imine})_2\text{O}_2\}$ chromophore with the elongation in the lateral chain¹⁸⁻²⁰. The $d-d$ transition bands due to the Co^{II} or Ni^{II} ion in **1**, **2**, **4**, **5**, **7** and **8** are not resolved.

Isomeric **6** and **10** are differentiated by visible spectra. The former has the superposed $d-d$ band of Cu^{II} at 617 nm (ϵ : 93 $\text{M}^{-1} \text{cm}^{-1}$), whereas the latter has the corresponding band maximum at 624 nm (ϵ : 103 $\text{M}^{-1} \text{cm}^{-1}$)³.

3.4c Cyclic voltammetry: The electrochemical properties of **1** ~ **9** were studied by cyclic voltammetry. Typical examples of cyclic voltammograms are given in figure 6, and the numerical data are summarized in table 7.

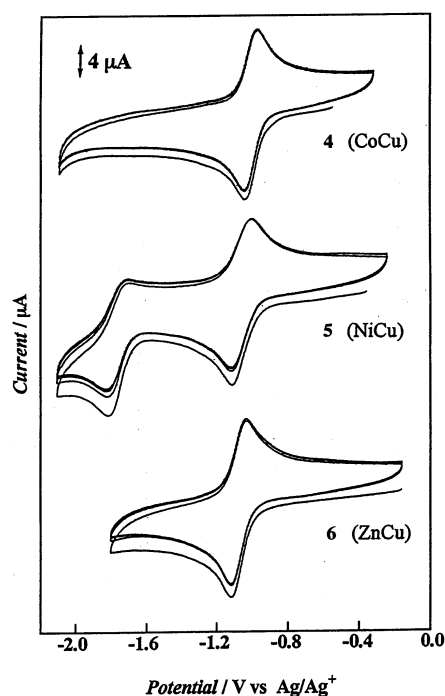


Figure 6. Cyclic voltammograms for **4**, **5** and **6**. Conditions for measurements are given in table 7.

Table 7. Electrochemical data for **1–10**.

Complexes	E_{pa}	E_{pc}	$E_{1/2}(DE)$	E_{pa}	E_{pc}	$E_{1/2}(DE)$
$[CoCu(L^{2:2})(AcO)]^{2+}$ (1)	-1.08	-1.19	-1.14 (0.11)			
$[NiCu(L^{2:2})(AcO)]^{2+}$ (2)	-1.10	-1.21	-1.16 (0.11)			
$[ZnCu(L^{2:2})(AcO)]^{2+}$ (3)	-1.26	-1.09	-1.18 (0.17)			
$[CoCu(L^{2:3})(AcO)]^{2+}$ (4)	-0.88	-0.96	-0.92 (0.08)			
$[NiCu(L^{2:3})(AcO)]^{2+}$ (5)	-0.92	-1.01	-0.95 (0.09)	-1.61	-1.71	-1.66 (0.10)
$[ZnCu(L^{2:3})(AcO)]^{2+}$ (6)	-0.95	-1.03	-0.99 (0.08)			
$[CoCu(L^{2:4})(AcO)]^{2+}$ (7)	-0.98	-1.07	-1.02 (0.09)			
$[NiCu(L^{2:4})(AcO)]^{2+}$ (8)	-0.97	-1.08	-1.03 (0.11)			
$[ZnCu(L^{2:4})(AcO)]^{2+}$ (9)	-0.91	-1.00	-0.96 (0.09)			
$[CuZn(L^{2:3})(AcO)]^{2+}$ (10)	-0.77	-0.85	-0.81 (0.08)			

Unit: V vs Ag/Ag^+ . Conditions: Glassy-carbon working, Pt auxiliary, and Ag/Ag^+ (TBAP/MeCN) reference electrodes. Supporting electrolyte: TBAP. Scan rate: 100 mV/s. Concentration: Complex (1×10^{-3} M), TBAP (1×10^{-1} M) in DMSO. $\Delta E = |E_{pa} - E_{pc}|$

In the sweep to negative potential, the complexes show a reversible or quasi-reversible couple at -1.05 ± 0.13 V (vs Ag/Ag^+) that is attributable to the Cu^{II}/Cu^I process in the iminic site²¹. Complex **5** (NiCu) with $(L^{2:3})^{2-}$ showed another reduction couple at -1.66 V that is attributed to the Ni^{II}/Ni^I reduction in the aminic site. For the other complexes, the reduction of the M^{II} was not observed in the available potential.

It must be emphasized that isomeric **6** and **10** differ in electrochemical property when compared under the same conditions. The former has the Cu^{II}/Cu^I couple at -0.99 V, whereas the latter has the corresponding couple at -0.81 V. The high Cu^{II}/Cu^I potential for the latter implies that the aminic site is more flexible to provide a non-planar environment preferred for Cu^I²².

3.4d *Magnetic properties:* The Zn^{II}Cu^{II} complexes (**3**, **6** and **9**) have a magnetic moment common for one unpaired electron (1.85, 1.86 and 1.83 μ_B , respectively). The magnetic moment of the Cu^{II}Zn^{II} complex **10** is reported to be 1.78 μ_B ³. The magnetic moments of the Co^{II}Cu^{II} complexes (**1**, **4** and **7**) and the Ni^{II}Cu^{II} complexes (**2**, **5** and **8**) are temperature-dependent, suggesting an antiferromagnetic spin-exchange interaction within each dinuclear unit. The $\chi_M T$ vs T plots for **1** and **2** are illustrated in figure 7.

The $\chi_M T$ value for **1** at room temperature is 2.68 K cm³ mol⁻¹ (4.63 μ_B) that decreased with decreasing temperature to 0.27 cm³ mol⁻¹ (1.48 μ_B) at 2.0 K. The moment at 2.0 K is lower than the spin-only value for $S_T = 1$ arising from the spin-coupling between Cu^{II} ($S = 1/2$) and Co^{II} ($S = 3/2$). This fact means the operation of secondary contribution(s) such as orbital effect and/or zero-field splitting of Co^{II}.

Magnetic simulations for **1** were carried out by the magnetic susceptibility equation for the ($S_{Co} = 3/2$) – ($S_{Cu} = 1/2$) system,

$$\chi_M T = \{N\mu_B^2/k(T - q)\} [10g_2^2 + 2g_1^2 \exp(-4J/kT)] / [5 + 3\exp(-4J/kT)] + Na, \quad (1)$$

where N is Avogadro's number, μ_B is the Bohr magneton, k is the Boltzmann constant, J is the exchange integral, T is the absolute temperature, q is the correction term for the

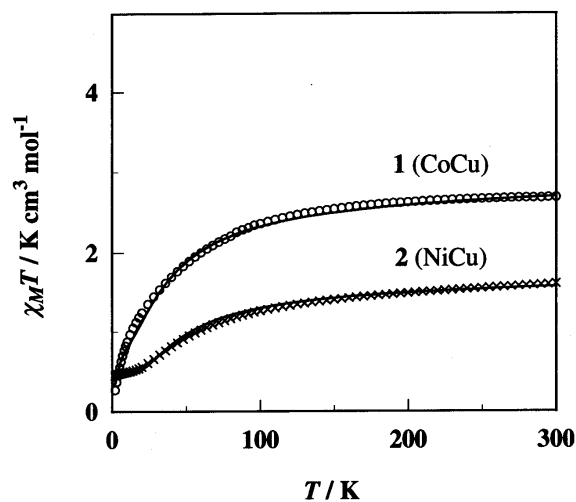


Figure 7. $\chi_M T$ vs T curves for **1** (trace a) and **2** (trace b). The solid curves are drawn based on the magnetic susceptibility expressions using the magnetic parameters given in the text.

secondary contribution(s), Na is the temperature-independent paramagnetism, and g_1 and g_2 are g factors associated with the total spin-states $S_T = 1$ and 2, respectively. The g factors are expressed using local g values (g_{Co} and g_{Cu}) as follows:^{23,24} $g_1 = (5g_{\text{Co}} - g_{\text{Cu}})/4$ and $g_2 = (3g_{\text{Co}} + g_{\text{Cu}})/4$. A good simulation was obtained as indicated by the solid line in figure 7, using the magnetic parameters $J = -10.0 \text{ cm}^{-1}$, $g_{\text{Co}} = 2.20$, $g_{\text{Cu}} = 2.10$, $q = -5.0 \text{ K}$, $Na = -300 \times 10^{-6} \text{ cm}^3 \text{ mol}^{-1}$. Similar magnetic simulations for **4** and **7** gave a negative exchange integral of -20.0 cm^{-1} and -9.0 cm^{-1} , respectively. It is notable that the $-J$ value for **7** is small relative to the values for **1** and **4**. The weak antiferromagnetic interaction for **7** is probably related to the distorted configuration about the Cu^{II} as previously discussed (see figure 4).

The $\chi_{\text{M}}T$ value for **2** at room temperature is $1.60 \text{ K cm}^3 \text{ mol}^{-1}$ ($= 3.46 \text{ mB}$) that decreased with decreasing temperature to $0.45 \text{ K cm}^3 \text{ mol}^{-1}$ (1.90 mB) at 2.0 K (figure 7, trace b). The magnetic moment at 2.0 K corresponds to the value for $S_T = 1/2$ resulting from spin-coupling between Cu^{II} ($S = 1/2$) and Ni^{II} ($S = 1$). Magnetic simulations were carried out using the magnetic susceptibility equation for the ($S_{\text{Ni}} = 1$) – ($S_{\text{Cu}} = 1/2$) system,

$$\chi_{\text{M}} = \{N\mu_{\text{B}}^2/4kT\} [10g_{3/2}^2 + g_{1/2}^2 \exp(-3 J/kT)] / [2 + \exp(-3 J/kT)] + Na, \quad (2)$$

where, $g_{1/2}$ and $g_{3/2}$ indicate the g factors associated with the total spin-states $S_T = 1/2$ and $3/2$, respectively, and other symbols have the same meanings as equation (1). The g factors are expressed using local g values as $g_{1/2} = (4g_{\text{Ni}} - g_{\text{Cu}})/3$ and $g_{3/2} = (2g_{\text{Ni}} + g_{\text{Cu}})/3$. The cryomagnetic property of **2** could be well reproduced by (2) as shown in figure 7, using the magnetic parameters of $J = -18 \text{ cm}^{-1}$, $g_{\text{Ni}} = 2.17$, $g_{\text{Cu}} = 2.10$ and $Na = 280 \times 10^{-6} \text{ cm}^3 \text{ mol}^{-1}$. Similarly, the exchange integrals for **5** and **8** were evaluated to be -25 and -33 cm^{-1} , respectively. Complex **2** shows a weak antiferromagnetic interaction compared with **5**. This can be explained by the large Ni displacement from the basal least-squares plane in **2** (0.721 \AA) compared with that for **5** (0.407 \AA).

4. Conclusions

A series of the (acetato) $\text{M}^{\text{II}}\text{Cu}^{\text{II}}$ complexes, $[\text{MCu}(\text{L}^{\text{m:n}})(\text{AcO})]\text{ClO}_4$ ($(\text{L}^{2:2})^{2-} \sim (\text{L}^{2:4})^{2-}$), were obtained from the mononuclear Cu^{II} precursors, $[\text{Cu}(\text{L}^{\text{m:n}})]$, and the site selectivity of metal ions was demonstrated by X-ray crystallography. The isomeric (acetato) $\text{Cu}^{\text{II}}\text{M}^{\text{II}}$ complexes, $[\text{CuM}(\text{L}^{\text{m:n}})(\text{AcO})]\text{ClO}_4$, could be prepared from the $\text{Pb}^{\text{II}}\text{Cu}^{\text{II}}$ precursors by taking advantage of the 'kinetic macrocyclic effect', but they were unstable to cause a scrambling of metal ions except for the case of $[\text{ZnCu}(\text{L}^{2:3})(\text{AcO})]\text{ClO}_4$. The coordination-position isomers, $[\text{ZnCu}(\text{L}^{2:3})(\text{AcO})]\text{ClO}_4$ and $[\text{CuZn}(\text{L}^{2:3})(\text{AcO})]\text{ClO}_4$, were differentiated by different physicochemical properties.

The core structures of $[\text{MCu}(\text{L}^{\text{m:n}})(\text{AcO})]\text{ClO}_4$ were studied in view of the ring-size of the macrocycle and the nature of the M^{II} ion. In $[\text{NiCu}(\text{L}^{2:2})(\text{AcO})]\text{ClO}_4 \cdot \text{MeOH}$, the Ni is largely displaced from the $\text{N}(\text{amine})_2\text{O}_2$ least-squares plane (0.721 \AA) and assumes a distorted six-coordination with a chelating acetate group. In $[\text{ZnCu}(\text{L}^{2:2})(\text{AcO})]\text{ClO}_4$, the acetate group bridges the metal ions because the Zn assumes five-coordination and the Zn displacement is smaller (0.66 \AA). The elongation of the lateral chain in the iminic site gives rise to a considerable adaptability for complexation not only for the iminic site but also for the aminic site. In $[\text{NiCu}(\text{L}^{2:3})(\text{AcO})]\text{ClO}_4$, the displacement of the Ni becomes small (0.407 \AA) to allow an acetate bridge between the metal ions. The macrocycle

$(L^{2:4})^{2-}$ has a higher adaptability for complexation as demonstrated for $[CoCu(L^{2:4})(AcO)(DMF)]ClO_4$, where the $N(amine)_2O_2$ moiety adopts a non-planar coordination mode providing a *cis*-octahedral configuration about the Co. On the other hand, $[ZnCu(L^{2:4})(AcO)]ClO_4$ has a (acetato) $Zn^{II}Cu^{II}$ core similar to that of $[NiCu(L^{2:3})(AcO)]ClO_4$ because Zn^{II} prefers five-coordination.

Acknowledgements

This work was supported by grants-in-aid for scientific research (No. 09440231), Scientific Research on Priority Area 'Metal-assembled Complexes' (No. 10149106) and an International Scientific Research Program (No. 09044093) from the Ministry of Education, Science and Culture, Japan. Thanks are also due to JSPS Research Fellowships for Young Scientists for support.

References

1. Ōkawa H, Furutachi H and Fenton D E 1998 *Coord. Chem. Rev.* **174** 51
2. Yonemura M, Matsumura Y, Ohba, Ōkawa H and Fenton D E 1996 *Chem. Lett.* 601
3. Yonemura M, Matsumura Y, Furutachi H, Ohba M, Ōkawa H and Fenton D E 1997 *Inorg. Chem.* **36** 2711
4. Yonemura M, Ohba M, Takahashi K, Ōkawa H and Fenton D E 1998 *Inorg. Chim. Acta* **283** 72
5. Fraser C, Johnston L, Rheingold A L, Haggerty B S, Williams G K, Whelan J and Bosnich B 1992 *Inorg. Chem.* **31** 1835; McCollum D G, Yap G P A, Rheingold A L and Bosnich B 1996 *J. Am. Chem. Soc.* **118** 1365 and references therein
6. Karunakaran B and Kandaswamy M 1994 *J. Chem. Soc., Dalton Trans.* 1595
7. Boudreaux E A and Mulay L N 1976 In *Theory and applications of molecular paramagnetism* (New York: Wiley) pp. 491–494
8. Cromer T D and Waber J T 1974 In *International tables for X-ray crystallography* (Birmingham, UK: Kynoch Press) vol IV
9. Ibers J A and Hamilton W C 1964 *Acta Crystallogr.* **17** 781
10. Creagh D C and McAuley W J 1992 In *International tables for crystallography* (ed.) A J C Wilson (Boston: Kluwer) pp. 219–222
11. Creagh D C and Hubbell H H 1992 In *International tables for crystallography* (ed.) A J C Wilson (Boston: Kluwer) pp. 200–206
12. TEXSAN 1985, 1992 Molecular Structure Corporation, Houston, Texas
13. Johnson C K 1976 Report ORNL-5138, Oak Ridge National Laboratory, Oak Ridge, Tennessee
14. Addison A W, Rao T N, Reedijk J, Rijn J V and Verschoor G C 1984 *J. Chem. Soc., Dalton Trans.* 1349
15. Deacon G B and Phillips R J 1980 *Coord. Chem. Rev.* **33** 227
16. Bosnich B 1968 *J. Am. Chem. Soc.* **90** 627
17. Downing R S and Urbach F L 1969 *J. Am. Chem. Soc.* **91** 5977
18. Ferguson J 1961 *J. Chem. Phys.* **34** 2206
19. Gruber S J, Harris C M and Sinn E 1968 *J. Inorg. Nucl. Chem.* **30** 1805
20. Xiong B, Song B, Zuo J, You X and Huang X 1995 *Polyhedron* **15** 903
21. Ōkawa H, Nishio J, Ohba M, Tadokoro M, Matsumoto N, Koikawa M, Kida S and Fenton D E 1993 *Inorg. Chem.* **32** 2949
22. Patterson G S and Holm R H 1974 *Bioinorg. Chem.* **4** 257
23. Chao C C 1973 *J. Magn. Resn.* **10** 1
24. Scaringe R P, Hodgson D J and Hatfield W W 1978 *Mol. Phys.* **35** 701